Pergamon

Int. J. Heat Mass Transfer. Vol. 40, No. 3, pp. 557–572, 1997
Copyright © 1996 Elsevier Science Ltd
Printed in Great Britain. All rights reserved
0017–9310/97 $15.00 + 0.00

PII: S0017–9310(96)00121–4

Heat transfer and ice formations deposited upon cold tube bundles immersed in flowing water—I. Convection analysis

PAUL ALEXANDER INTEMANN and MICHAEL KAZMIERCZAK†

Department of Mechanical, Industrial and Nuclear Engineering, University of Cincinnati, Cincinnati, OH 45221-0072, U.S.A.

(*Received* 1 *December* 1995 *and in final form* 29 *March* 1996)

Abstract—A staggered and an in-line tube bank configuration were subjected to a crossflow of water. Internal tube subcooling ($< 0°C$) resulted in gradual ice deposits to occur on the outside of the tubes; this moving ice–water interface was then allowed to stabilize. Testing focused on the low to moderate Reynolds number range ($Re = 100$–1300) and ice–water cooling temperature ratios Θ between 0.5 and 8. Photographic documentation was followed by a finite element analysis (FEA) of each ice shape. Steady-state results included (1) the total rate of energy exchange Q between the tubes and the crossflow, (2) the total ice volume V which eventually coats the tubes, and (3) the row-to-row variation of both Q and V within the tube banks. Steady-state ice shape contours observed fell into three different categories: (1) thin, almost concentric ice formations (high Reynolds and/or low Θ values); (2) elongated ice shapes with a dominant axis either parallel or perpendicular to the crossflow; and (3) large ice deposits connecting adjacent tubes and leading to ice bridging of varying extent (low Reynolds and/or high Θ values). The ice formations will, when compared to non-icing tube banks at similar Reynolds numbers, either increase or decrease the heat transfer rates depending upon the volume of ice accumulated. Correlations for Nusselt number and the total amount of ice volume produced on both staggered and in-line tube banks with ice formations at steady state were developed. Copyright © 1996 Elsevier Science Ltd.

INTRODUCTION

The increasing demand for advanced building cooling systems that are both economical and environmentally friendly has led to the development of various new types of thermal energy storage devices, some of which operate on the principle of utilizing the latent heat of phase change associated with water in order to obtain their specified cold storage capacity requirements. Systems which function based upon this water phase-change phenomena can generally be categorized into three different hardware storage configurations: ice-on-tube designs, ice module designs, and ice harvesters. The ice storage method most widely utilized today is of the first kind: it essentially consists of pipes, submerged in a crossflow of cold water, that are refrigerated sufficiently to cause ice formations to be deposited upon the tubes' exteriors. Not surprisingly, the growing popularity of these systems has resulted in a substantial increase, particularly during the past two decades, in the research efforts dealing with the phenomena of forced convective freezing of ice on the exterior of isolated and multi-subcooled tubes. Although many previous investigators have studied the thermal-hydrodynamic characteristics associated with tube banks *without* phase change, only relatively recently has the combination of subcooled refrigerated tubes arranged in a true geometric tube bank configuration been approached.

Due to the well-established flow complexities documented in tube-bank flow fields, research activities investigating the performance characteristics of tube bundle heat exchangers have been mostly experimental. A century of work has resulted in a thorough and exhaustive understanding of tube bank heat exchanger performance capabilities, with probably the two most complete studies of their kind being carried out be Grimison [1] and Zukauskas and Ulinskas [2]. Simultaneously, the study of solid–liquid phase change heat transfer has historically been focused primarily on investigating *conduction* phase change heat transfer processes; this was generally achieved by studying problems occurring in either stagnant fluids or with simple geometries exposed to flow fields that could be modeled with a uniform convective film coefficient, thus significantly limiting the impact and importance of the convective heat transfer conditions of many realistic problems. Unfortunately, the complex flow patterns which exist in tube bank flow fields do not readily allow for this over-simplification; convection in these cases is as important in driving the heat transfer as is conduction. In fact, many researchers who have investigated *convective* freezing with far less complex flow fields have discovered that,

† Author to whom correspondence should be addressed.

NOMENCLATURE

A	clean tube bank total exterior surface area [cm^2]
a	s_t/d
b	s_l/d
b'	s_l'/d
d	copper tube outside diameter, 1.7145 cm
k	thermal conductivity [W m^{-1} K^{-1}]
K_f	dimensionless heat transfer parameter, equation (5)
Nu	average experimental Nusselt number, equation (3)
Pr	Prandtl number, υ/α
Q	heat transfer rate [W]
R^2	statistical multiple coefficient of determination
$Re_{d,max}$	Reynolds number, equation (1)
s_t	transverse distance between adjacent tube centerlines [cm]
s_l	streamwise longitudinal distance between adjacent tube centerlines [cm]
s_l'	relative longitudinal distance between adjacent tube centerlines [cm]
T	temperature [K]
U	velocity [cm s^{-1}]
V	ice volume [cm^3]
V^*	non-dimensional ice volume, equation (4).

Greek symbols

α	thermal diffusivity [cm^2 s^{-1}]
Θ	cooling temperature ratio, equation (2)
μ	dynamic viscosity [g cm^{-1} s^{-1}]
υ	kinematic viscosity [cm^2 s^{-1}]
ρ	fluid density [g cm^{-3}].

Subscripts

f	ice–water interface
ice	total ice within tube bank
max	maximum
row	tubes perpendicular to the water crossflow
tubes	all tubes comprising a bank
w	tube wall surface
∞	fluid (water).

under certain conditions, the interaction between the resulting solid–liquid interface's spatial location and the surrounding liquid flow field may be so strong that only a coupled solution to the problem would yield reasonable results [3, 4]. This paper investigates exactly such a problem, where the mutual dependence between the interface and the external flow field *must* be taken into account.

A significant number of convective freezing studies focusing on icing of *single* or *dual cylinder* arrangements in a crossflow of water have been reported [5–7]. Icing in multiple cylinders (tube banks) were first reported by Okada *et al.* [8], who explored the ice formations associated with a *staggered* tube bank in a water crossflow. Their analysis included a graphical depiction of the transiently growing ice–water interface, as well as documentation, using an FEA approach, of the circumferential variation of the local convective heat transfer coefficient between different tubes within the tube bank. They concluded that the heat transfer from tubes with ice layers is almost the same as that for staggered cylinders without ice. That study was followed by Hirata and Matsui [9], who investigated the ice formation phenomena around a *single line* of isothermally subcooled cylinders. Torikoshi *et al.* [10, 11] then investigated the formation of ice around horizontally mounted tubes in both *in-line* and *staggered arrangements*, unfortunately all freezing experiments were conducted without any forced crossflow occurring past the tubes. Finally, Hirata and Matsui [12] published a study of both staggered and in-line arrangements in which they reported the global heat transfer of isothermally cooled cylinders exposed to a forced crossflow of water. In contrast to Okada *et al.*'s staggered tube bank arrangements, it can be argued that the experimental arrangements used by Hirata and Matsui [12] did not exactly constitute a fully fledged tube bank design, but in effect consisted of a *single line* of tubes flanked on either side by semi-cylindrical tubes rigidly attached to the bounding walls of the test facility, however their study did represent the first attempt to investigate the forced convective freezing within an *in-line* subcooled cylinder arrangement. More recently, Intemann and Kazmierczak [13] investigated the heat transfer performance of tubes with icing in both staggered and in-line tube bank configurations utilizing 16-tubes in a four rows by four columns geometric configurations. Those experiments resulted in the generation of two new empirical heat transfer correlating equations which were based upon experimental heat transfer data inferred from an overall system energy balance.

The results presented in Part I of the current study focuses on the *global aspects* (i.e. overall heat transfer, total ice volume, ice linkage, etc.) of the phase-change phenomenon as it occurs within the confines of real tube bank configurations from a convection heat transfer point of view, while Part II continues the analysis by investigating the convection phenomenon close-up, i.e. locally, which eventually led us towards

an altogether different approach in analyzing the icing problem.

EXPERIMENTAL APPARATUS

All experiments were performed in the experimental freezing/melting water tunnel shown schematically in Fig. 1a. The experimental setup as shown consists of four major sub-systems: the water tunnel and its flow control, the test section, the cooled tube bank, and the data acquisition and process control equipment. A detailed description of the water-tunnel hardware configuration and flow control may be found in Intemann and Kazmierczak [13].

Tunnel test section

The freezing of water took place within the subcooled tube banks positioned inside the water-tunnel test section. The dimensions of this test section measure 25.4 cm high by 12.7 cm deep by 38.1 cm long. The front and rear sides of the test section included a pair of removable windows; each test configuration essentially consisted of two new windows with a custom-made hole pattern which were used to rigidly hold the tubes in place during testing. One set, with a staggered hole arrangement (Fig. 1b), and another, with an in-line hole arrangement (Fig. 1c), were machined to study the geometric impact of tube arrangement on the resulting ice formations and heat transfer. Double-layered Plexiglas was used in the test section to minimize heat migration into the test section and to prevent condensation on exterior observation surfaces.

Tube banks and tubes

Both tube banks tested consisted of 16 tubes. All tubes were manufactured using a commercially available thick-walled copper pipe (0.675 in o.d.). To initiate ice formations on the tubes' exterior, all tubes were cooled internally, in parallel, to below the fusion temperature of water. A double annular tube design (bayonet configuration), which allowed single-sided coolant-supply (50/50 glycol–water mixture) entry into and exit out of the tubes, was used to facilitate unimpeded viewing of the tube banks and resulting ice formations during the experiments.

Tube bank heat transfer rate and ice volumes determination

A relatively simple, yet tedious, energy balance method, taking into account all external energy influences on the global water tunnel, was initially used to determine the global heat transfer rate which occurred through the ice-encrusted tube banks. Results based on this methodology were previously reported by Intemann and Kazmierczak [13]. Unfortunately, a determination of the resultant steady-state ice *volumes* was not possible utilizing this method, nor could the individual contribution to Q by selected tubes be determined. The current study, which is aimed at determining both Q_{bank} and the non-dimensional ice volume V^* (total amount and spatial variation of such) deposited on the tubes at steady state, required a new and different approach to achieve its goals. Thus, a finite element analysis routine of the ice formations was adopted to satisfy all required test objectives. In essence, it consisted of the following: after an experiment had reached steady state, all tube bank configurations were first documented photographically by taking close-up end-view exposures of the resulting ice shapes. The resulting end-view contour images were then digitally scanned and imported into appropriate digitizing software. Here, the tube–ice and ice–water interface contours were converted into digital data files. The ice boundary temperature conditions were also known at both interfaces, the ice–water interface temperature was 0°C while the tube–ice interface temperature was obtained from the thermocouples imbedded in the tube walls. Thus, based on both the known end-view geometric ice contours and the temperature boundary conditions, a finite element analysis (FEA) of each individual ice shape was initiated.

The digitized ice boundary contours and temperatures were input into the ANSYS® Rev. 5.0 general purpose finite element computer program. The mesh generation of the ice shape was accomplished utilizing a two-dimensional four-node plane element with thermal conduction capabilities, resulting in the analysis essentially solving the steady-state two-dimensional heat conduction equation within the end-view ice shapes. Each ice shape was modeled using a total of 1080 elements; grid checks in both the radial and the circumferential directions were performed to verify the sufficiency of the chosen 1080 element grid density [14]. Output from each FEA run consisted of the following: the total Q transferred across the ice layer of each tube–ice combination, the total end-view cross-sectional area of the ice layer surrounding each tube, and, based upon the freestream temperature of the crossflow, the local convective heat transfer coefficient along the perimeter of the ice–water interface. The total heat transfer rate and ice volume of the entire tube bank could thus easily be determined by summing up all of the Qs and Vs of the 16 individual tubes, as determined by the FEA runs, within the bank at a particular experimental test condition.

EXPERIMENTAL PROCEDURE AND DATA REDUCTION

All steady-state experiments followed the same basic procedure. Initially, a plate heat exchanger was valved "in" as part of the facility and the low-temperature chiller was used to lower the tunnel water temperature until it read approximately 2–3°C. This typically took anywhere from 1 to 2 h. After this, the plate heat exchanger was valved "out" and the chiller glycol–water temperature was reset to a new value. This new chiller set temperature was dependent upon

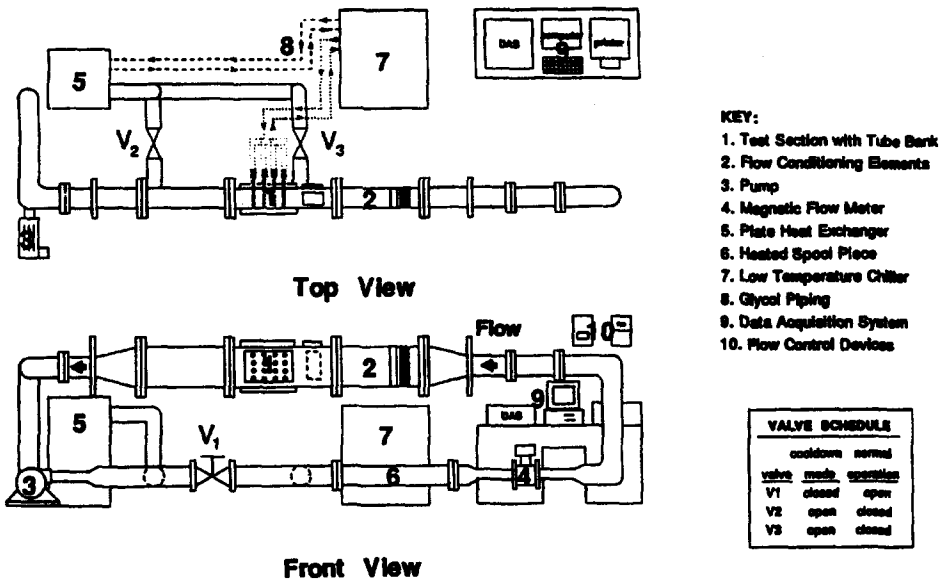

(a)

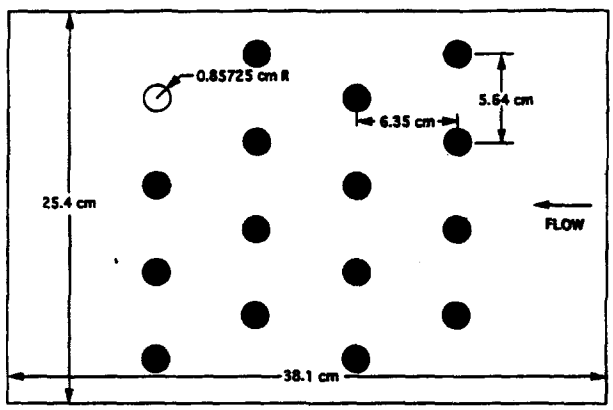

(b)

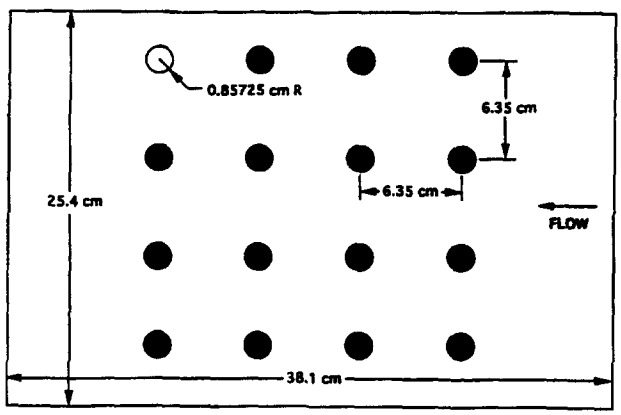

(c)

Fig. 1. Ice-on-tube bank experimental test equipment. (a) Sketch of freezing water tunnel facility; (b) staggered tube bank arrangement showing dimensions; (c) in-line tube bank arrangement showing dimensions.

the desired cooling temperature ratio Θ of the upcoming test. Once this new value was achieved, the glycol–water mixture was then redirected to circulate through the tube bank to cool down the tubes and begin the freezing process. Initially the ice grew rapidly, but this slowed significantly with time. Eventually, when $Q_{\text{conduction}} = Q_{\text{convection}}$ at the ice–water interface, the ice growth stopped and steady-state conditions prevailed. The length of time it took for the system to achieve steady-state conditions varied somewhat depending on the imposed test conditions, but in general 12–18 h were usually sufficient to allow the system to stabilize. At that point, the data was logged by the data acquisition system and the end-view photographs of the ice shapes were taken. This data was then input into a spreadsheet program which calculated the following two dimensionless input parameters: the Reynolds number $Re_{d,max}$ of each experiment based upon the freestream flow conditions and the maximum fluid velocity within the tube bank; and the non-dimensional cooling temperature ratio Θ, a measure of the amount of ice subcooling relative to the crossflow water superheating,

$$Re_{d,max} = \frac{\rho U_{max} d}{\mu} \tag{1}$$

$$\Theta = \frac{(T_f - T_w)}{(T_\infty - T_f)}. \tag{2}$$

The results of the FEA analysis were then used to obtain the following desired dimensionless output parameters: the average tube bank Nusselt number Nu; and the dimensionless ice volume V^* for each experiment,

$$Nu = \frac{Q_{\text{tubes}} \times d}{k_\infty A(T_\infty - T_f)} \tag{3}$$

$$V^* = \frac{V_{\text{ice}}}{V_{\text{tubes}}}. \tag{4}$$

Finally, to facilitate comparison of these results with *non-icing* tube bank correlations developed by earlier investigators, the average tube bank Nusselt number (equation (3)) was then converted to a K_f number, a parameter similar to a Nusselt number but modified by removal of the fluid's Prandtl number dependence defined as:

$$K_f = \frac{Nu}{Pr_\infty^{0.36}(Pr_\infty/Pr_f)^{0.25}} \tag{5}$$

where the assumed values of the exponents are the accepted empirically constants from the work of Zukauskas and Ulinskas [2].

Uncertainty analysis

The procedure presented by Moffat [15] applicable to single-sample experimental data collection and reduction was implemented to obtain a measure of the uncertainty in the reported results for $Re_{d,max}$ and K_f. The typical uncertainty associated with the Reynolds number, spanning all 43 experimental data points collected, was determined to be approximately 1.3%. The average uncertainty in K_f was found to be roughly 10%; note that these results include both bias and random errors of the measured variables. The possible sources of error in the reported Reynolds numbers included the water flow velocity uncertainty, the tube diameter measurement accuracy, and the inherent 'fossilized' error in the reference water viscosity. The uncertainty in K_f arises from possible errors in the numerous variables used in calculating its final value, as well as the accuracy of the FEA analysis, while the freestream water temperature and tube surface thermocouple uncertainties *were* both included (note, ice–water interface digitizing accuracy and photographic stigmatic lens distortion are examples of some of the potential sources of errors that were not considered in the uncertainty analysis).

RESULTS AND DISCUSSION

Characteristic ice shapes

Perhaps the first and most important information obtained by the early investigators of conventional ("non-icing") tube bank designs was that performance characteristics between staggered and in-line tube bank designs differed *significantly*. This statement likewise applies to ice-on-tube bank designs: not only were the observed heat transfer characteristics of the two designs significantly different, but the ice shapes themselves which formed were also very different and distinct in both total ice volume and interface shapes. These differences between the banks became even more pronounced and exaggerated as the dimensionless cooling temperature ratio Θ was increased. In general, the ice shapes *within* the staggered tube bank configuration were found to usually grow predominately in a transverse direction relative to the crossflow (see Fig. 2a, photograph) and exhibit a minimum ice layer thickness at their forward stagnation point. The location of this minimum thickness is believed to be due to the direct impingement of water after it has exited through the upstream flow constriction formed by two other adjacent ice-coated tubes. In contrast, the in-line tube bank ice shapes were found to generally assume an elongated shape in the streamwise direction where the maximum ice thickness was found to line up parallel with the direction of the freestream flow (see Fig. 2b photograph). This exaggerated growth phenomena, which became even more pronounced with increasing Θ values, is attributed to a combination of the increased 'shadowing effect' due to upstream tubes with larger Θs and the resulting, relatively calm, re-circulation zones upstream and downstream of tubes which are located within the interior of the in-line tube bank.

The above-mentioned elongation phenomenon observed with both tube bank geometries, more

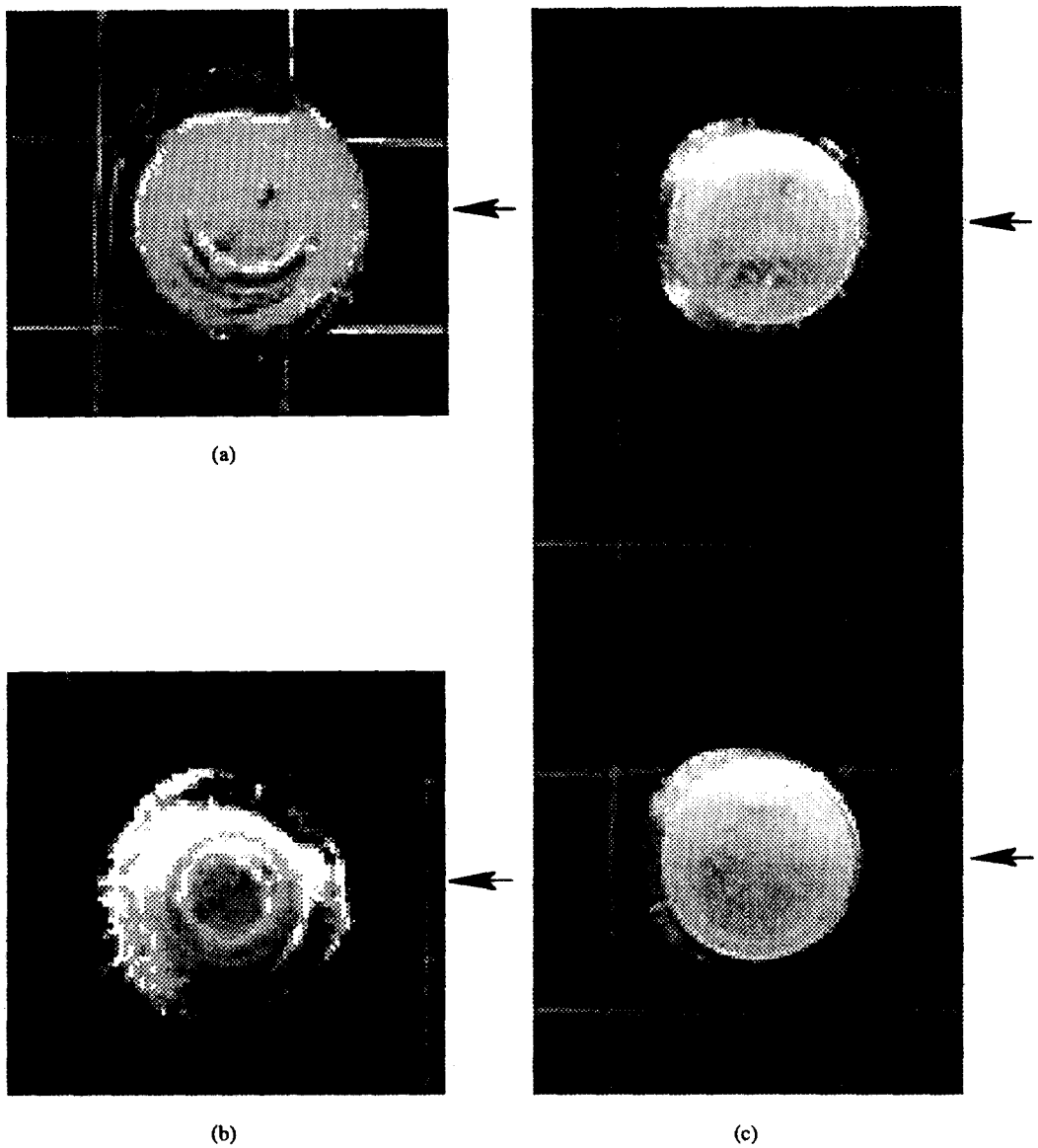

Fig. 2. Photographs of typical ice shapes. (a) Staggered configuration showing transverse ice elongation ($Re_{d,max} = 1000$, $\Theta = 8$); (b) in-line configuration showing longitudinal ice elongation ($Re_{d,max} = 660$, $\Theta = 8$), (c) in-line experiment number 22: high Reynolds number, low Θ ($Re_{d,max} = 1000$, $\Theta = 1$).

closely depicted by the digitized ice shapes and plotted for a variety of different test condition, are shown in Fig. 3. While Fig. 3a represents the ice shape contour variation of a Row 3 tube with varying Reynolds number (for fixed $\Theta = 4$) with the staggered tube bank configuration, the contour plots in Fig. 3b are for a Row 3 tube with changing Θ (for fixed $Re_{d,max} = 300$) for the in-line tube bank configuration. The difference in primary ice growth direction, either transverse or longitudinal, between the two tube bank geometries is obvious. The gradual transverse ice contour elongation with decreasing Re exhibited by the tube in the staggered tube bank is in sharp contrast to the primary longitudinal ice growth direction observed on the tube located within the in-line tube arrangement.

After examining all of the end-view photographs taken during this study, the following additional general ice shape category was also noted; ice shapes which were thin and almost concentric with a somewhat flattened rear surface area. This was documented for both the staggered and the in-line tube bank configurations alike and was found in experiments that were performed which involved a combination of low Θ and high Reynolds numbers. See Fig. 2c for a photograph of a representative ice contour belonging in this category. Finally, with regards to ice shape characterization, one last observation worth men-

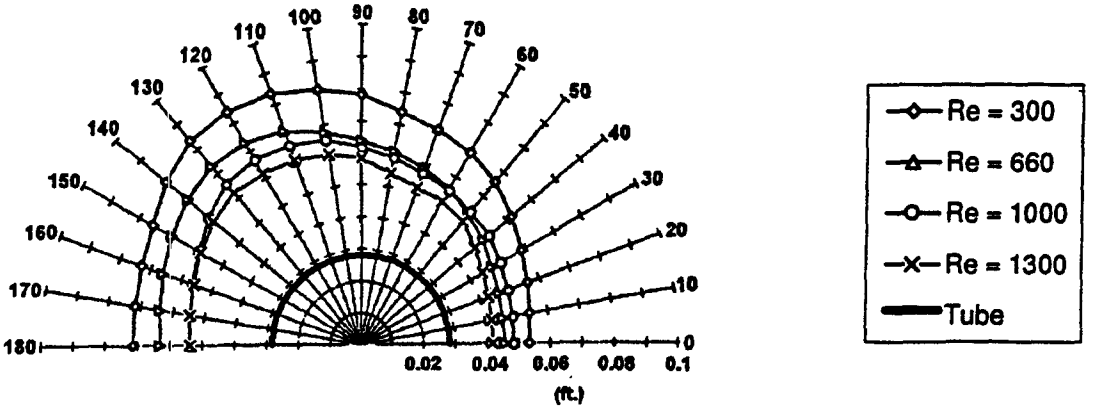

(a)

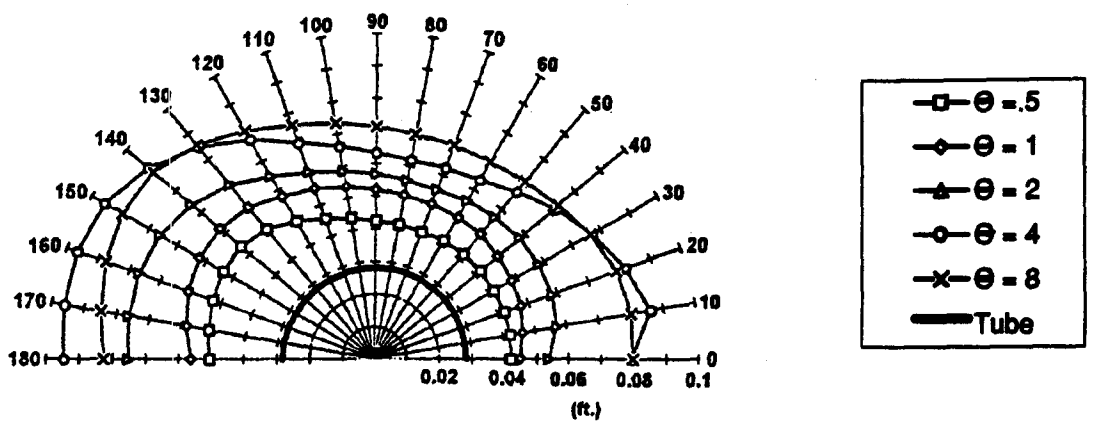

(b)

Fig. 3. Circumferential ice interface position of tubes located in Row 3 of the tube banks. (a) Staggered configuration: radial variation as a function of Reynolds number at $\Theta = 4$; (b) in-line configuration, radial variation as a function of Θ at $Re_{d,max} = 300$.

tioning is that, for experiments which produced large ice deposits, the ice shapes which formed around the tubes located in the very first and last rows of the tube bank were noticeably different from those observed within the interior of the bank; this was presumably due to the physical absence of any upstream and downstream tube bank rows, and their associated non-impact in altering the bypass entrance and exit flow patterns relating to these particular tubes located in the first and last rows. See Intemann [14] for further details.

Global tube bank heat transfer and ice volume

Staggered arrangement. The staggered tube bank arrangement was tested by performing a total of 20 steady-state experiments; both the Reynolds number

Table 1. Freezing tube bank results

Experiment	Conditions	$Re_{d,max}$	Θ	K_f	V^*	Linkage
		(a) Staggered arrangement				
1	170/0.5	176	0.50	4.11	1.50	N
2	170/1	173	1.09	6.28	2.74	N
3	170/2	172	2.09	9.51	4.31	N
4	170/4	171	4.06	14.10	7.39	N
5	170/8	176	5.56	10.30	15.78	Y
6	300/0.5	301	0.48	3.97	1.50	N
7	300/1	302	1.10	7.08	2.20	N
8	300/2	293	1.89	9.54	3.31	N
9	300/4	306	4.21	16.36	5.88	N
10	300/8	298	8.26	24.10	10.64	Y
11	430/1	467	1.04	6.76	2.16	N
12	430/2	430	2.00	10.35	3.27	N
13	430/8	438	8.48	27.32	8.65	Y
14	660/4	691	4.14	19.50	4.02	N
15	660/8	664	8.35	29.90	6.69	N
16	1000/4	1009	4.31	22.93	3.45	N
17	1000/8	1014	7.99	34.91	5.17	N
18	1300/1	1298	1.04	10.04	1.34	N
19	1300/2	1322	2.06	17.02	1.69	N
20	1300/4	1298	3.68	23.59	2.62	N
		(b) In-line arrangement				
1	170/0.5	172	0.50	3.48	1.83	N
2	170/1	168	0.97	4.96	3.26	N
3	170/2	162	2.08	6.62	9.30	Y
4	170/4	165	4.03	8.92	13.07	Y
5	170/8	170	5.18	9.71	17.08	Y
6	300/0.5	284	0.50	3.62	1.68	N
7	300/1	285	1.00	5.93	2.38	N
8	300/2	282	1.96	8.76	3.87	N
9	300/4	286	3.94	12.17	9.56	Y
10	300/8	288	8.42	21.14	14.47	Y
11	430/0.5	429	0.47	3.91	1.35	N
12	430/1	424	0.98	6.86	1.79	N
13	430/2	414	2.01	10.09	3.17	N
14	430/4	414	4.01	13.87	7.39	Y
15	430/8	418	7.89	21.7	12.64	Y
16	660/0.5	671	0.50	3.54	1.20	N
17	660/1	665	1.00	7.59	1.56	N
18	660/2	650	2.01	11.72	2.43	N
19	660/4	658	3.93	16.34	4.47	N
20	660/8	632	6.07	21.1	6.50	N
21	1000/0.5	989	0.51	5.12	1.06	N
22	1000/1	977	0.98	8.56	1.32	N
23	1000/2	943	1.97	13.27	1.95	N

and the dimensionless cooling temperature ratio Θ constituted the test parameters which were varied between the individual experiments. Reynolds numbers between 170 and 1300 and Θ values from 0.5 to 8 were included. The summation of the FEA analysis of the individual ice shapes resulted in both the total tube bank heat transfer rates, expressed as K_f according to equation (5), and the total non-dimensional ice volumes V^*, as expressed by equation (4), for the complete tube bank. These results are reported in Table 1a and are graphically displayed in Fig. 4. As is apparent from Fig. 4a, an increase in both of the primary test parameters, Reynolds number and Θ will result in an increase in the global heat transfer rate of the staggered tube bank. The difference in the heat transfer rates between the experimental results obtained here with ice formations, and those for clean tube banks without ice coatings reported by Zukauskas and Ulinskas [2] are obvious and striking. The tube bank heat transfer rate with ice build-up is much less than the non-icing tube bank heat transfer (solid line in Fig. 4a) for low values of Θ, but increases significantly over that of a non-icing tube bank as the Θ ratio increases. The single exception to this trend seems to be the results obtained from experiment 5; it should be noted that this particular test point resulted in 13 of 16 tubes within the bank linking together to form a single solid ice configuration. (Further discussion into the affect of ice linkage on tube bank performance and predictive relations is included later in this study.) The analysis of the ice volumes collected resulted in an opposite trend to that observed

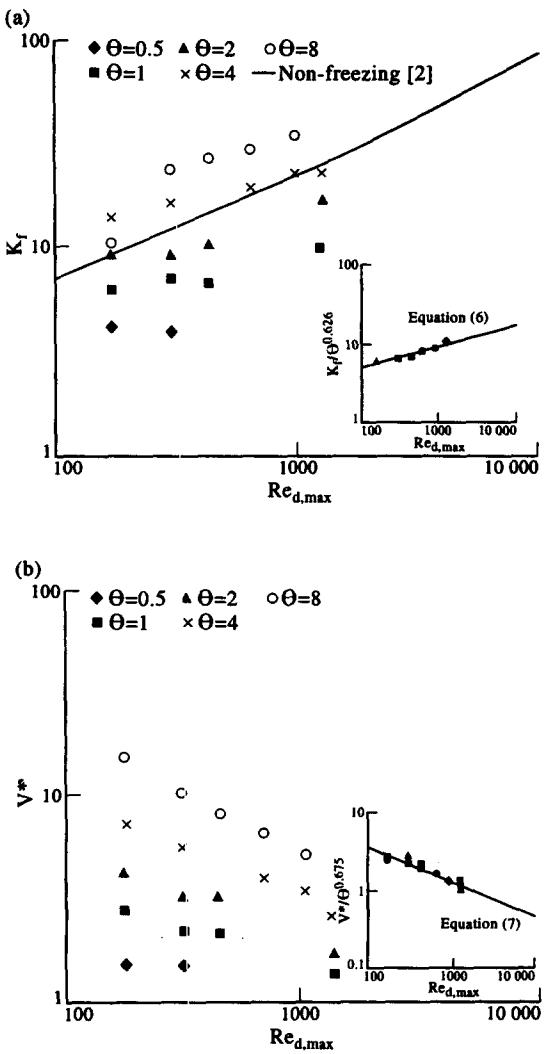

Fig. 4. Staggered freezing tube bank results. (a) Total bank heat transfer rate; (b) total ice volume.

for K_f (see Fig. 4b); now a rise in the Θ value and a *decrease* in the Reynolds number was found to drive up the amount of ice which formed upon the tube's exterior surfaces.

A statistical analysis of this heat transfer and ice volume data was performed to obtain appropriate correlating equations which would best describe the observed experimental steady-state data trends. Previous correlating equations derived to describe non-icing tube bank performance predictions, such as those developed by Zukauskas and Ulinskas [2], would appear to be an appropriate platform to build upon; therefore a similar equation "structure" was almost expected and thus examined, but with the obvious inclusion of the Θ parameter. Equation (6) below, which fits the data with a multiple coefficient of determination R^2 of 0.992, was generated for the staggered tube bank data (experiment 5 excluded) obtained during this study:

$$K_f = 1.449 \times Re_{d,max}^{0.267} \times \Theta^{0.626}. \quad (6)$$

This equation is plotted as the solid line in the lower insert of Fig. 4a and shows very good agreement with the experimental test data. The same type of statistical analysis was carried out for the dimensionless ice volume data V^* and resulted in

$$V^* = 23.734 \times \frac{\Theta^{0.675}}{Re_{d,max}^{0.418}}. \quad (7)$$

The data fit of this correlation was almost as good as the K_f correlation; the test data was found to collapse quite nicely upon the line represented by the V^* correlating equation depicted in the lower right hand corner of Fig. 4b and has a multiple coefficient of determination R^2 of 0.980.

Note that the above heat transfer trends observed here are in sharp contrast to those reported earlier by Okada *et al.* [8]. Their heat transfer test data, expressed as experimentally derived Nusselt numbers when plotted based upon idealized 'circular' ice diameters and corrected for flowpath blockage effects, was found to essentially blanket the range *between* the non-icing heat transfer correlations for staggered tube banks *and* a single tube in a crossflow, causing them to conclude that a staggered tube bank *with* ice exhibits nearly the same Nusselt number–Reynolds number relationship as tube banks *without* ice. A simple reanalysis of our test data, based upon the same 'circular' ice diameter and flowpath blockage correction, did not resolve these differences however. Our data, when plotted in this manner, showed that the staggered tube bank's heat transfer rates with ice deposits were now, on average, 63% lower than those predicted by the Zukauskas and Ulinskas non-icing staggered tube bank correlations and 50% lower than the non-icing single tube correlation, and thus represent results which are significantly different from those reported by Okada *et al.* Curiously, a further comparison between the limited steady-state ice volumes reported by Okada *et al.* and those tabulated in Table 1a of this study showed that Okada *et al.*'s test runs produced, at comparable test conditions (*Re* and Θ), approximately 73% *less* ice volume than was obtained with our test facility. The reasons for these differences are unresolved at this time, but, we suspect, could be attributed to any one of a number of factors, including differences in the quality of the inlet flow field (non-uniformity/turbulence levels), as well as accuracy of Reynolds number and Θ measurements between the two different testing facilities.

In-line arrangement. Next, the in-line tube bank was installed in the water tunnel and 23 steady-state experiments were conducted. The range of Θ values under which this configuration was tested exactly mirrored that used for the staggered arrangement, while the freestream flow conditions were slightly altered to include Reynolds numbers ranging between 170 and 1000. A summary of the heat transfer rates K_f and ice volumes V^* for this arrangement is given in Table 1b

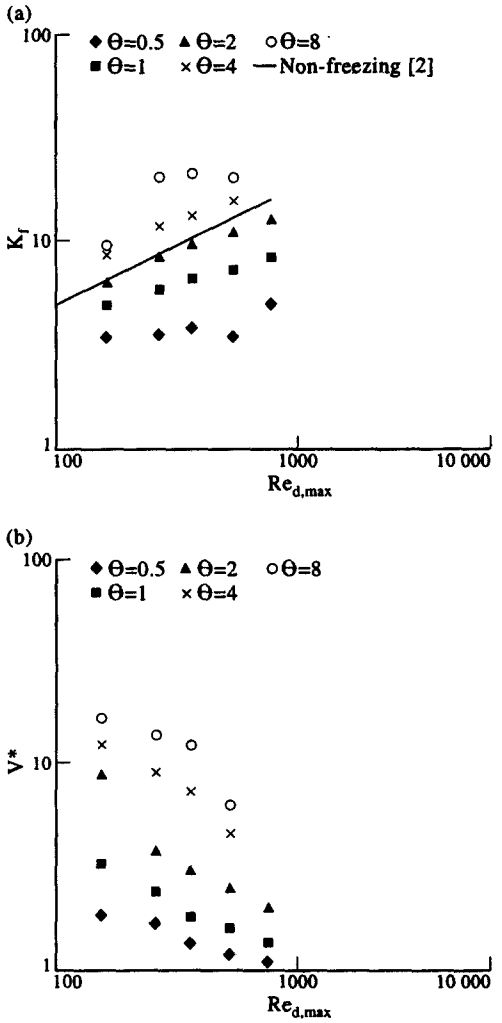

Fig. 5. In-line freezing tube bank results. (a) Total bank heat transfer rate; (b) total ice volume.

and is plotted in Fig. 5. Once again, the data shows a significant variance in the magnitude of heat transfer when compared to the correlation developed by Zukauskas *et al.* for in-line tube banks without icing, although the deviation is not as large as previously obtained for the staggered tube bank arrangement. The heat transfer data plotted in Fig. 5a exhibits the same basic behavior as was observed for the staggered bank array, i.e. K_f is seen to increase with Θ, but falls below the non-freezing baseline for small values of Θ and above it for larger Θs. The large K_f values at high Θ ratios may seem somewhat surprising, since this is exactly the conditions at which the in-line tube bank exhibits significant ice-linkage between adjacent tubes. One explanation to account for this may be the trade-off between the decrease in K_f due to the 'shadowing' effect which occurs in in-line tube bank configuration and the increase in K_f due to the resultant enhanced 'channel flow' in the narrowed passages formed by linked or almost-linked tube bank columns. The rise in the convective heat transfer rate along such 'wavy plates' formed by adjacent ice linkage [12] may be sufficient to more than offset the simultaneous decrease in heat transfer due to this ice bridging and thus could be responsible for elevating the K_f values at high Θ ratios above the established non-freezing baseline without ice formations. Regarding the ice volume performance (Fig. 5b), experiments conducted on the in-line tube bank unmistakably showed that, compared to the staggered arrangement, the in-line tube bank has a much greater affinity to link via ice bridging, and therefore produces a significantly larger ice volume at identical test conditions. For example, comparing the resulting V^* of experiment 4 of the staggered and in-line tube banks in Table 1a and b, respectively, shows that the ice linkage nearly doubles the ice volume at these identical test conditions.

As before, a statistical analysis of the in-line experimental data was performed. All data points, *including* those which exhibited ice bridging between adjacent tubes, were included in deriving the correlations. The equations found to best fit the in-line tube experimental data were as follows:

$$K_f = 1.085 \times Re_{d,max}^{0.291} \times \Theta^{0.612}, \quad (R^2 = 0.976) \quad (8)$$

$$V^* = 94.247 \times \frac{\Theta^{0.803}}{Re_{d,max}^{0.621}}, \quad (R^2 = 0.938). \quad (9)$$

Comparing the correlations developed for the staggered and in-line tube banks together, shows that, at least for the K_f parameter, the impact of the Θ parameter for the in-line tube bank with ice formation and the staggered tube bank with ice formations is roughly equal; 0.612 (equation (8)) vs 0.626 (equation (6)). On the other hand, the ice volume correlations are not as comparable to one another; not only is the coefficient of the equation for the in-line arrangement roughly four times greater than that of the staggered arrangement, but the exponent of the Θ parameter on the resultant ice volume of an in-line tube configuration is significantly larger than that for the staggered tube bank arrangement. Thus, it may be fair to summarize that the documented variations of K_f and V^* for the two tube geometries investigated show similar trends, but differ significantly in magnitude, at identical $Re_{d,max}$ and Θ test conditions.

Effect of tube row location

Previously published non-icing tube bank performance studies by both Grimison [1] and Zukauskas and Ulinskas [2] have suggested that the initial two rows in a tube bank configuration through which the incoming fluid must first traverse, exhibit heat transfer characteristics which are significantly different, i.e. lower, than the remaining downstream tube rows (rows 3 and beyond). General consensus is that the initial rows act as turbulence generators, thereby increasing the heat transfer of the later tubes. More-

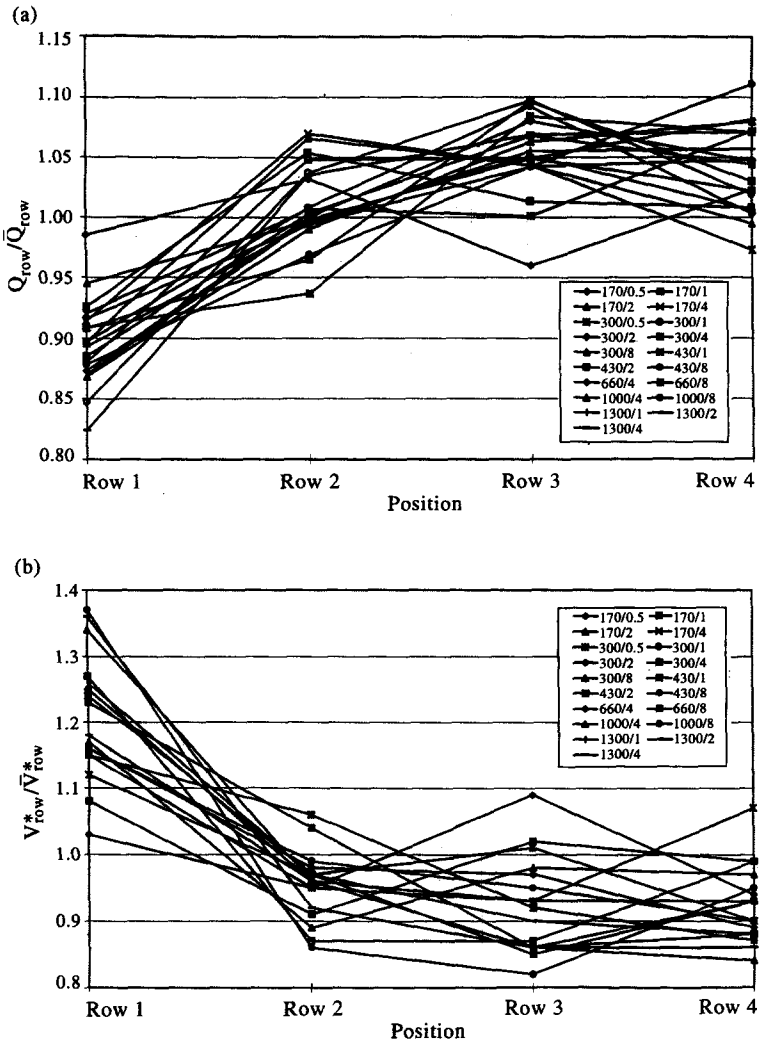

Fig. 6. Staggered freezing tube bank row variation results. (a) Heat transfer; (b) ice volume.

over, it has been observed that the heat transfer rate from successive rows tends to stabilize and becomes constant once the flow has penetrated sufficiently deep into the interior of the bank (beyond the second row). In-line tube banks *with* small longitudinal pitch ratios seem to be the only exception to this rule, where the tight tube spacing leads to the previously discussed 'shadowing effect', leading to decreased heat transfer rates with row depth.

Staggered arrangement. The steady-state heat transfer rate of the staggered tube bank arrangement with ice formations used in this study clearly exhibited this expected increasing performance behavior with row location; i.e. Q_{row} was seen to increase with bank penetration which then levels off. Figure 6a shows the variation of Q_{row} with tube bank location for all experiments carried out with the staggered tube bank array, non-dimensionalized by the average $\bar{Q}_{row}$ heat transfer rate defined as:

$$\bar{Q}_{row} = \frac{\sum_{1}^{4} Q_{row}}{4}. \tag{10}$$

Although the magnitudes of these spatial variances were found to be highly dependent on both the Reynolds number and the Θ parameter, the general upward trend in the heat transfer effectiveness of rows located further inside the tube bank's interior is unmistakable. As expected, for most experiments, the increase in Q_{row} is greatest from row one to row two, it diminishes with penetration depth and then tends to disappear. The heat transfer rate exhibited by the fourth row is somewhat mixed when compared to the preceding third row; this is not totally unexpected since it is essentially the last row of the configuration and therefore cannot really be qualified as an internal row. The effect of tube location on the ice volumes collected within each row was also studied. Fig. 6b,

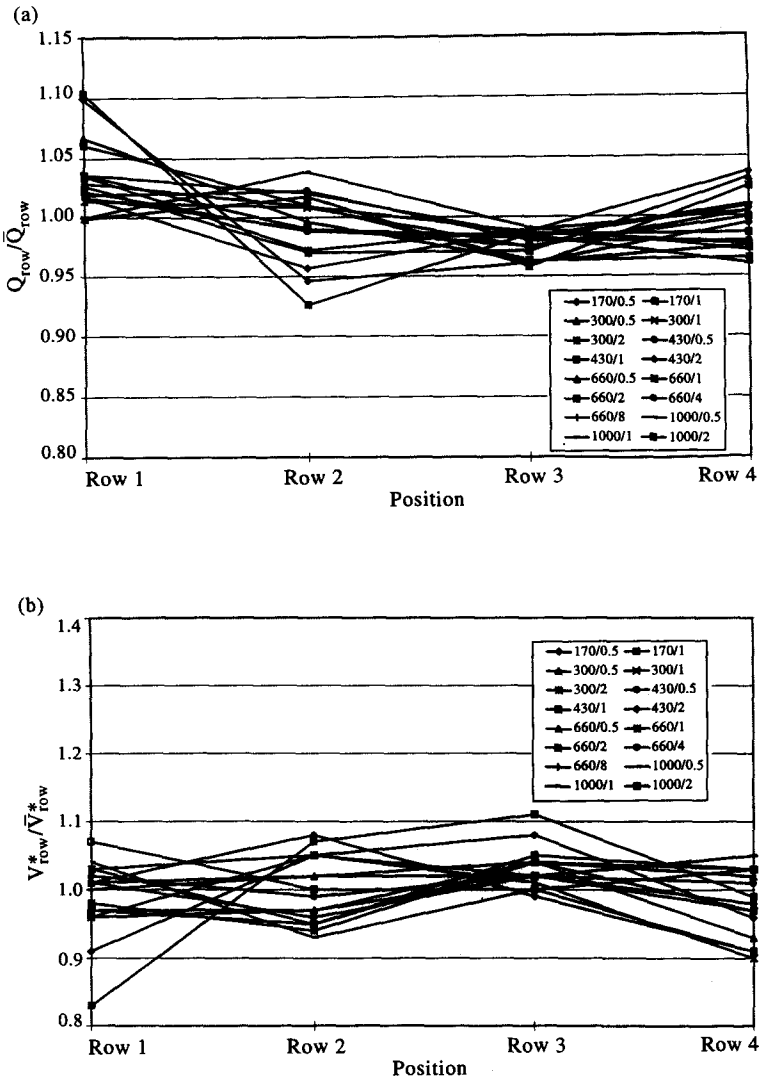

Fig. 7. In-line non-linking freezing tube bank row variation results. (a) Heat transfer; (b) ice volume.

where V^*_{row} replaces Q_{row}, indicates that the volume of ice which is deposited upon the tubes within successive rows clearly decreases and, similarly to Q_{row}, flattens out between rows 3 and 4; but note again, there are some exceptions. These results support the conclusion that ice volume and heat transfer rate for a given tube bank *row* follow an inverse relationship, i.e. that lower heat transfer rates mean more ice accumulation and vice-versa.

In-line arrangement. The spatial variation of Q_{row} and V^*_{row} of the in-line tube bank arrangement was generally opposite to that observed for the staggered tube bank configuration; the row-to-row dependence of the in-line experiments without ice bridging is shown in Fig. 7. Results show that for almost all Reynolds numbers and Θ values tested, the in-line tube bank performed contrary to what was expected, i.e. the spatial variation of Q_{row} showed a consistent decrease with row location; a fact not altogether surprising, since our data also unmistakably showed that the ice formations that appear at most Θ values have the tendency to *decrease* the effective longitudinal pitch ratio of the configuration, thereby driving down the heat transfer from row-to-row as the fluid penetrates into the in-line test tube bank design. The variation of Q_{row} with row location, where Q_{row} is again compared to the performance of an average row, is shown in Fig. 7a, while the ice volume variation from row-to-row is shown in Fig. 7b and is found to behave inversely with its heat transfer variation.

Tube–ice linkage

While numerous experiments of both the staggered and in-line test configurations resulted in ice linkage to occur between adjacent tubes within the banks, the frequency of this observed ice bridging was found to be highly dependent upon the tube bank configuration type. As the last column of Table 1 shows, the in-line bank had a much higher propensity to exhibit linked ice tubes than its staggered tube bank counterpart; a

tendency which is not at all surprising, considering the resulting internal flow structure of these two different tube bank geometries.

Staggered arrangement. As expected, the staggered arrangement did not exhibit a great tendency for ice bridging; this is due primarily to the inherent flow field surrounding each tube brought about by the geometric constraints of the staggered configuration. If ice bridging within the staggered arrangement were to occur, the most likely site of such linkage would be the diagonal opening between the first two rows of tubes, i.e. along the relative longitudinal pitch of the bank. Indeed, two experiments did result in such very limited partial ice bridging between adjacent tubes (Fig. 8). In one case (experiment 13), two diagonal tubes connected, while in the other (experiment 10) two *pairs* of diagonal tubes connected. In both cases the connection occurred between tubes in the first row of the bank and a diagonally positioned tube in the second row, which according to Figure 6a is the location of lowest heat transfer and hence greatest ice volume build-up within such a bank. It is interesting to note that the impact of these minor linkages are not readily discernible in terms of the global K_f and V^* values reported in Fig. 4. However, the one run mentioned earlier (experiment 5) which resulted in a steady-state configuration where a significant number of tubes were linked together (13 of 16 tubes totally connected) did exhibit a significantly lower global tube bank heat transfer rate than expected when compared to the trend of K_f values for the remaining staggered tube bank experiments. This data point was clearly seen to fall out of line in Fig. 4a. Thus, the occurrence of ice linkage between adjacent tubes, while it certainly increases the total ice volume which is deposited within the tube bank confines, was seen, in at least one case, to adversely affect the heat transfer characteristics of the staggered tube bank configuration. Therefore, a method which could predict a minimum tube bank pitch, and insure no ice linkage for a given set of test conditions would occur, was highly desirable. Determination of this critical pitch, to predict the minimum tube spacing necessary to just initiate contact between adjacent ice tubes, was thus developed based upon the ice volume correlations assuming an idealized cylindrical ice shape and geometric reasoning. It is given by the following equation:

$$P_{crit} = \sqrt{1 + V^*} \tag{11}$$

where V^* depends on Reynolds number and Θ through equation (7).

The actual diagonal pitch of the tested staggered tube bank was 4.05, which is indicated by the solid line in Fig. 9a along with the P_{crit} for the V^* values obtained for each staggered tube bank experiment. The three solid data points shown in Fig. 9a are the three staggered tube bank experiments where partial ice linkage was observed to occur; the uppermost data point, the experiments in which a large ice block was seen to form within the tube bank configuration, is seen to essentially fall on top of the horizontal line representing the actual tube bank pitch of 4.05. Thus, for design purposes, one can conclude that equation (11), in conjunction with equation (7), can be used to estimate the minimum relative longitudinal (diagonal) pitch required to inhibit significant adjacent ice bridging within staggered tube bank configurations.

In-line arrangement. A total of *six* experiments utilizing the in-line tube bank arrangement resulted in either partial or total linkage of tubes located within one or more columns; this compared to only three experiments that exhibited ice linkage in the staggered tube bank arrangement. Also note that tube linkage in the in-line tube bank was always found to connect tubes that were aligned in the longitudinal direction, i.e. were parallel to the water flow direction; linkage between tubes located within the same row occurred only once, during experiment 5. Figure 8b is a photograph of an experiment which shows tubes that have partially or completely linked in the streamwise direction to effectively redirect the crossflow water into separate passages of a 'multi-channel flow' configuration. The greater tendency for tubes in the in-line bank to link is clearly a result of the 'shadowing' effect, a flow condition much more prevalent in the in-line configuration than in the staggered tube bank arrangement; with increasing Θ, as the growth of ice on the previous rows of tubes becomes large, the downstream tubes are effectively shielded from the water flow and resigned to sit in regions of fluid with low velocities; a condition itself conducive to further ice growth. This enhanced rate of ice building further drives the shadowing phenomena; until adjacent tubes within the same column will eventually connect. It is interesting to note that the occurrence of significant ice linkage within the in-line tube bank geometry does *not* seem to adversely affect the trend in K_f, as can be seen from Fig. 5.

Similar to the staggered configuration, a tube linkage criteria, but this time based on the streamwise longitudinal distance between tubes, was also developed and tested for the in-line arrangement. Figure 9b again shows the P_{crit} results for each measured V^* from the in-line tube bank experiments; the actual longitudinal pitch ratio of the in-line tube bank was 3.70. As can be seen, the six experiments (solid symbols) which resulted in some or significant ice bridging are all seen to gradually approach and even exceed (with enhanced linkage the higher up one moves) the line representing the actual pitch of the test configuration. Thus, once again, equation (11), but this time in conjunction with equation (9), which represents the applicable ice volume correlation to use for in-line bank configurations, can be used to estimate the minimum longitudinal pitch necessary to preclude the occurrence of adjacent tube ice bridging in such in-line tube bank configurations.

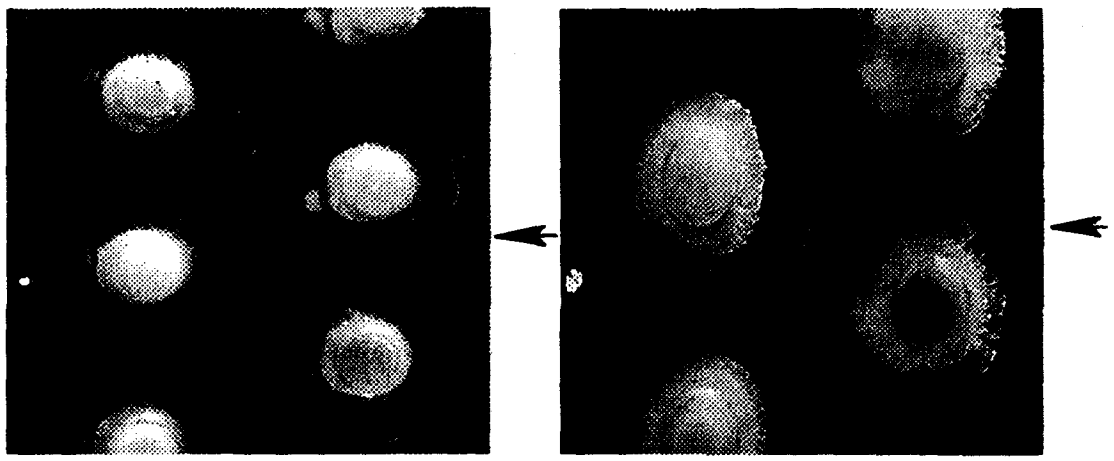

(a)

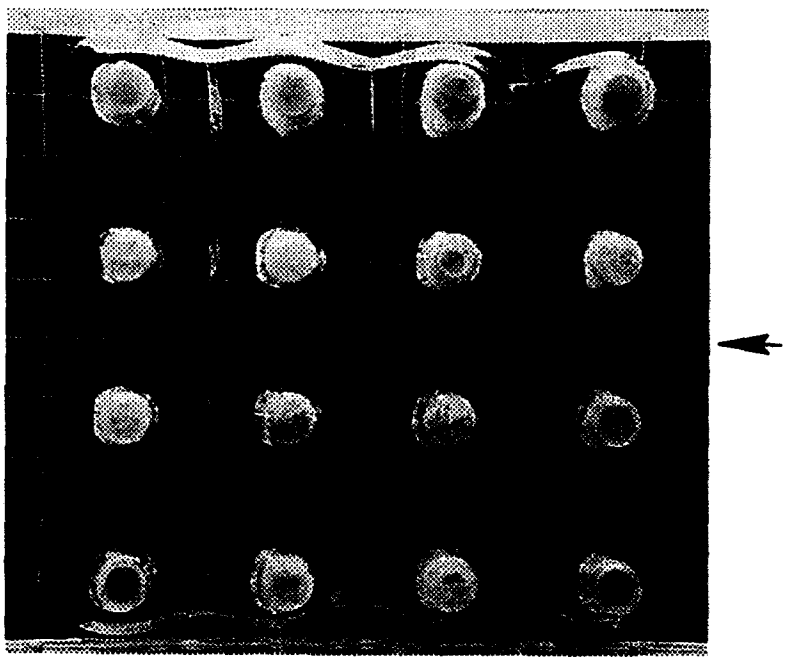

(b)

Fig. 8. Freezing experiments with ice linkage. (a) Staggered tube bank; experiment 10 (left photograph) showing two diagonal tube pairs linked, experiment 13 (right photograph) showing single diagonal tube pair linked. (b) In-line tube bank; experiment 3. Note the partial ice linkage between rows 1 and 2 due to the increased heat transfer rate of the front row.

CONCLUSIONS

A total of 43 steady-state forced convection ice-on-tube experiments were conducted using both a 16-tube staggered and a 16-tube in-line bank arrangement. Each of the two configurations was found to possess pluses and minuses; the staggered arrangement was better than the in-line configuration in its ability to function as an effective heat exchanger, while the in-line configuration was superior in its ability to maximize the total ice volume deposited upon the tube walls. More specifically, at identical Reynolds numbers and Θ values, the staggered arrangement was between 18 and 58% more effective than the in-line configuration in its ability to perform as a heat exchanger. The ice linkage phenomenon in the staggered arrangement, when it was found to occur, changed drastically, by going from a condition of little or no ice bridging, to a condition of a large ice block connecting 80% of the tubes with gradual changes in

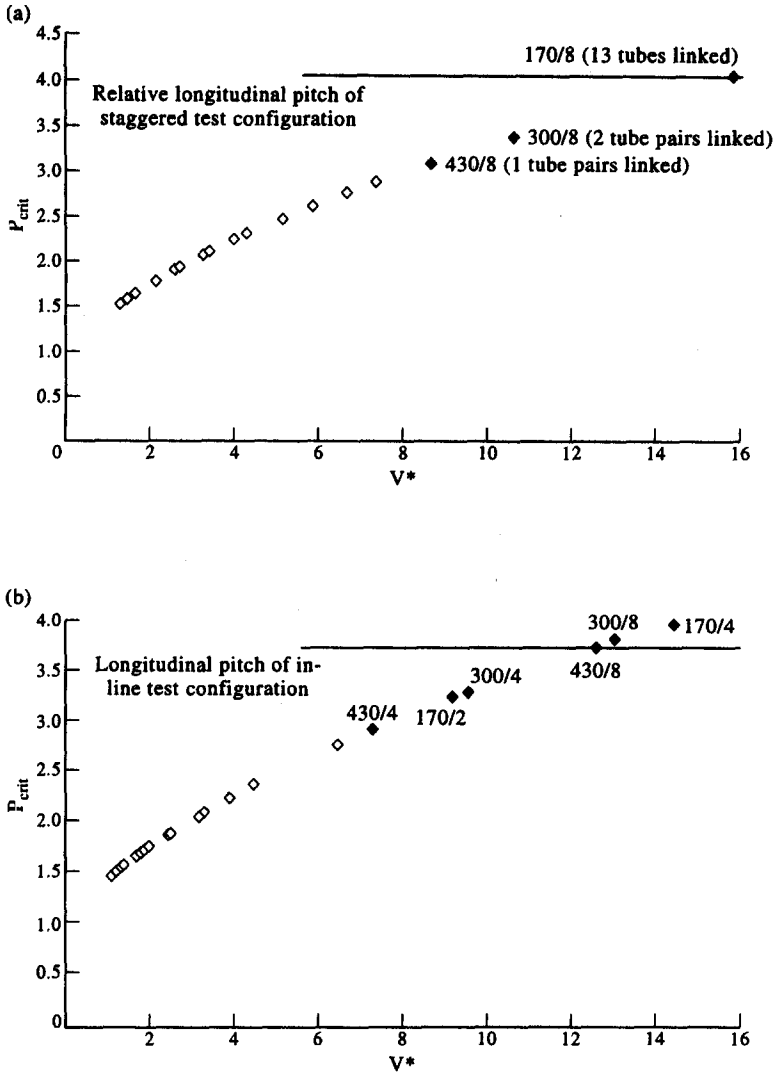

Fig. 9. Freezing tube bank ice linkage critical pitch results. (a) Staggered arrangement; (b) in-line arrangement.

the $Re_{d,max}$ and Θ parameters. In contrast, the ice linkage behavior, with varying $Re_{d,max}$ and Θ, of the in-line tube bank configuration was much more gradual and resulted in a much greater range of different ice linkage combinations.

The study also resulted in various correlations to quantify the effect of ice coating within tube bank configurations from a convective heat transfer and total ice volume point of view. Design of future ice-on-tube phase change devices should significantly benefit from these steady-state heat transfer and ice volume correlations, expressed as functions of $Re_{d,max}$ and Θ, for in-line and staggered tube bank geometries. Additionally, the influence of tube spatial positioning within a tube bank geometry was investigated and significant differences between the in-line and staggered bank arrangements were found. Finally, by utilizing the total ice volume correlations, a methodology to preclude adjacent tube ice bridging by ensuring adequate tube pitch was developed for both geometries of interest, and substantiated with the experimental data.

As is typical in most research endeavors, many more new questions were raised in the process of analyzing a given problem. This study was no exception to the rule. A comparison of the heat transfer performance characteristics exhibited by the staggered tube bank configuration tested here with previously reported data by Okada *et al.* has resulted in many additional questions; the most obvious being: why did Okada *et al.* report a negligible effect of the ice layer on the tube bank heat transfer rate when our data indicate otherwise? In addition, if our data are accurate, the large spread in the experimental K_f values which we obtained is also somewhat surprising. Finally, how does one account for the fact that small Θs were detrimental to the overall tube bank heat transfer rate, while experiments with higher Θ values, i.e. larger ice

build-up on the tubes, tended to increase the heat transfer capabilities of both arrangements beyond that of similar geometry non-icing tube banks? An analysis of the *local* heat transfer behavior of *individual* tubes within the banks, across the range of different Reynolds numbers and Θ values tested, might possibly reveal the answers to many of these questions; and will, together with other additional aspects of this problem, be thoroughly addressed in Part II of this study.

REFERENCES

1. E. D. Grimison, Correlation and utilization of new data on flow resistance and heat transfer for cross flow of gases over tube banks, *Trans. ASME* **59,** 583–594 (1937).
2. A. Zukauskas and R. Ulinskas, *Heat Transfer in Tube Banks in Crossflow*, Chap. 3. Hemisphere, New York (1988).
3. M. Epstein and F. B. Cheung, Complex freezing–melting interfaces in fluid flow, *A. Rev. Fluid Mech.* **15,** 293–319 (1983).
4. F. B. Cheung and M. Epstein, Solidification and melting in fluid flow, *Adv. Transport Process.* **3,** 35–117 (1984).
5. M. Okada, K. Katayama, K. Terasaki, M. Akimoto and K. Mabune, Freezing around a cooled pipe in crossflow, *Bull. JSME* **21,** 1514–1520 (1978).
6. K. C. Cheng, H. Inaba and R. R. Gilpin, An experimental investigation of ice formation around an isothermally cooled cylinder in crossflow, *J. Heat Transfer* **103,** 733–737 (1981).
7. G. S. H. Lock and T. M. V. Kaiser, Icing on submerged tubes: a study of occlusion, *Int. J. Heat Mass Transfer* **28,** 1689–1698 (1985).
8. M. Okada, K. Gotoh and S. Nakamura, Ice formation on a tube bank (in Japanese), Report on Research and Survey of Heat Pump Technology, Japanese Association of Refrigeration, pp. 49–68 (1987).
9. T. Hirata and H. Matsui, Ice formation and heat transfer with water flow around isothermally cooled cylinders arranged in a line, *ASME J. Heat Transfer* **112,** 707–713 (1990).
10. K. Torikoshi, Y. Nakazawa and H. Yamashita, *An Experimental Study of Formation and Melting of Ice About Horizontal Tubes*, Vol. HTD 143, pp. 57–63. ASME, New York (1990).
11. K. Torikoshi and Y. Nakazawa, *An Experimental Study of Formation and Melting of Ice around Horizontal Tubes: Influence of Tubes Array on Ice Formation and Melting Characteristics*, Vol. HTD 205, pp. 19–25. ASME, New York (1992).
12. T. Hirata and H. Matsui, Freezing and thawing heat transfer with water flow around isothermally cooled cylinders in staggered and aligned arrangements, *ASME J. Heat Transfer* **114,** 681–687 (1992).
13. P. A. Intemann and M. Kazmierczak, Convective heat transfer for cold tube bundles with ice formations in a stream of water at steady state, *Int. J. Heat Fluid Flow* **15**(6), 491–500 (1994).
14. P. A. Intemann, Steady and transient forced convective freezing experiments on subcooled tube bundles in a crossflow of water, Ph.D. thesis, University of Cincinnati, Cincinnati, OH (1996).
15. R. J. Moffat, Describing the uncertainties in experimental results, *Expl Thermal Fluid Sci.* **1,** 3–17 (1988).